A Scalable Numerical Framework for Predicting Particle Transport in Bifurcating Vascular Networks

Md Zaheen Tamzeed Kabir[1] and Jon McCullough[1][0000-0002-9606-0408]

[1] Queen's University Belfast, University Road, Belfast, Northern Ireland, BT7 1NN, UK
mkabir01@qub.ac.uk
jon.mccullough@qub.ac.uk

Abstract. Cardiovascular diseases remain the predominant cause of death worldwide. Although computational fluid dynamics is an effective tool for predicting hemodynamics and drug particle transport in arteries, its clinical adoption remains limited due to the complexity of the workflow and computational limitations. This paper presents a scalable approach for predicting hemodynamic parameters and particle exit fractions in large networks from results obtained for ideal bifurcations. A total of 828 3D CFD simulations, combined with particle tracking, were performed on a high-performance computing environment with variations of inlet velocity, particle density, inlet and outlet diameters, and bifurcation angles on Y and T-shaped bifurcations. The simulation dataset was used to train three ML algorithms: Linear Regression, k-Nearest Neighbour, and Random Forest Regression for the prediction of velocity and particle exit fraction at the bifurcation outlets. Larger vascular networks were built by successively combining predictions from single bifurcation variants, thereby reducing computational costs. Our model successfully predicted the distributions of particle exit fraction and velocity in larger networks with better accuracy and reduced runtime than a 1D model of a realistic hepatic artery geometry and a reconstructed model.

Keywords: Machine Learning (ML), Computational Fluid Dynamics (CFD), Bifurcating Vessels, Multiscale Modelling, Lagrangian Particle Tracking (LPT)

1 Introduction

Approximately 523 million people worldwide suffer from cardiovascular disease (CVD), resulting in a significant public health burden and a primary cause of illness and death in all age divisions [1]. Personalised therapies remain one of the significant challenges in drug delivery applications, notably in treating CVDs, primarily due to the complexity of an individual's vascular structure [2]. Computational Fluid Dynamics (CFD) has been widely used by clinical researchers to predict the behaviour of blood flow and drug particle deposition in arteries, which would be highly difficult to obtain experimentally [3,4]. However, the application of CFD in clinical settings remains limited largely due to high computational costs, limitations in MRI/CT image segmentation, and data protection policies [5,6].

ICCS Camera Ready Version 2026
To cite this paper please use the final published version:
DOI: 10.1007/978-3-032-29915-4_1

In recent times, CFD coupled with data-driven machine learning (ML) or deep learning (DL) has proven to be an alternative to overcome computational costs. A CFD-ML approach developed by Malek et al. [7] investigated left coronary artery (LCA) bifurcations with varying stenosis severity and location using computational fluid dynamics (CFD) to calculate hemodynamic parameters. A dataset of 6,858 synthetic coronary artery geometries was generated, and fourteen machine learning regression models were trained using the CFD-derived results. Among these models, the Decision Tree Regressor and K-Nearest Neighbour showed the best performance for predicting total average wall shear stress (TAWSS) and oscillatory shear Index (OSI), closely matching the CFD outputs. Another similar approach was found in blood flow modelling of a simplified 2D vessel containing magnetic nanocarriers for cancer therapy. The CFD-derived data were used to train machine learning models predict fluid velocity [8]. One study that combines CFD with the discrete element method (DEM) for resolving suspended particles and ML techniques was reported by Islam et al. [9]. Here, the authors performed coupled CFD–DEM simulations of pharmaceutical aerosol flow in both idealised and realistic airway models to capture the interaction between the continuum phase (airflow) and the discrete phase (particles). Similar to the work of [9], Francis et al. [10] performed CFD simulations of particle transport in an acinar region of the lung to determine the striking velocity and impact time for three particle diameters under both healthy and diseased (high surface tension) conditions in lung airways. The resulting CFD data for these two hemodynamic parameters were used to train machine learning classifiers that accurately identified the optimal particle diameter required to achieve desirable striking velocities and impact times. Lin et al. [11] performed 3D CFD simulations on 1,000 subject-specific aortic geometries. The authors investigated the distributions of velocity, pressure, and wall shear stress (WSS). The authors then trained deep neural networks on the CFD outputs to predict velocity magnitude and direction, pressure, and WSS for unseen geometries. The prediction models in their study were further compared against an additional 100 geometries and showed good agreement (deviation of 3-5%). In an attempt to reduce computation time, 1D segmentation of coronary vessels combined with an ML approach was applied by Coenen et al. [12] for predicting fractional flow reserve for diagnosing CVDs, reducing computational time by 5 – 10 minutes per patient. Another attempt to reduce computation was made by Ko et al. [13]. One-dimensional flow and pressure distributions were predicted using a reduced-order fluid model in coronary trees.

Although CFD coupled with an ML/DL approach is a promising way to reduce computational time, it also requires substantial time to run simulations on larger vascular networks and to generate the training dataset. Furthermore, it is extremely difficult to obtain such a dataset without substantial simplification of the underlying physics, which might omit critical information of interest [14,15]. For example, 1D models homogenise the flow profile across a domain, leading to a failure to capture local particle deposition [14].

In this paper, we introduce a scalable approach for predicting flow behavior and particle transport in large vascular networks based on CFD with particle tracking and ML. Conceptually, CFD results for flow and particle transport in a single bifurcation are used to train an ML model, reducing the complexity of generating this dataset.

ICCS Camera Ready Version 2026
To cite this paper please use the final published version:
DOI: 10.1007/978-3-032-29915-4_1

Larger networks are then efficiently constructed by chaining together multiple bifurcation variants. Figures 1 and 2 outline the steps taken by this approach.

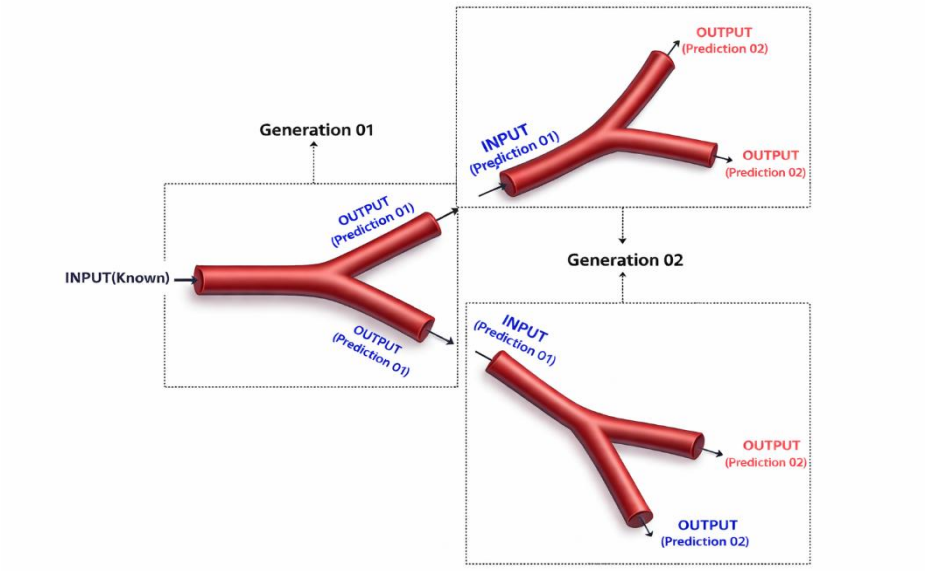

Fig. 1. Graphical overview of our multiscale model for predicting flow in large networks

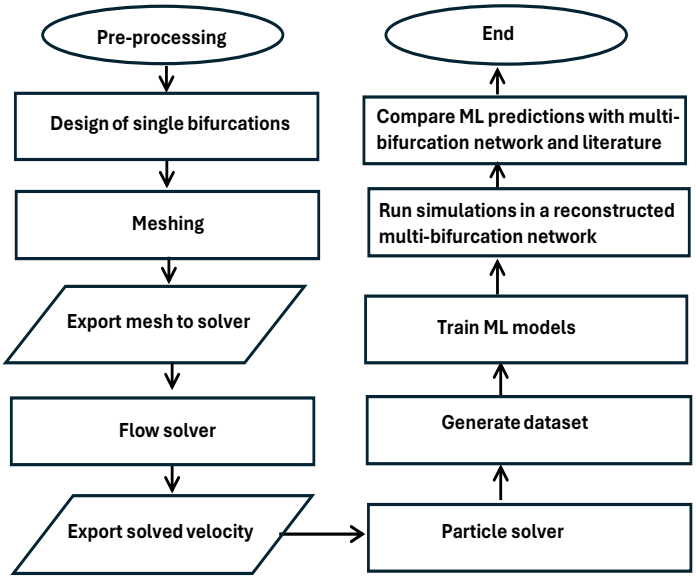

Fig. 2. The systematic workflow of the complete methodology for predicting particle trajectories in large networks

ICCS Camera Ready Version 2026
To cite this paper please use the final published version:
DOI: 10.1007/978-3-032-29915-4_1

2 Methodology

The workflow for the current study is presented in Figure 2. A total of 93 geometries with varying parameters of Y and T bifurcations were constructed using SOLIDWORKS 2024 [16]. The numerical simulations were performed on the compute nodes of the NI-HPC high-performance computing (HPC) cluster Kelvin2 [17]. The CFD simulations were performed using an open-source CFD software, OpenFOAM version 8.0 [18]. The ML models were trained using an open-source Python library, scikit learn [19].

2.1 Governing Equations

2.1.1 Modelling Blood Flow.

The incompressible, steady, laminar momentum and continuity equations were numerically solved using the finite volume method (FVM) for modelling blood flow.

$$\rho_f \left(\frac{\partial \vec{v}_f}{\partial t} + \vec{v}_f . \nabla \vec{v}_f\right) = -\overrightarrow{\nabla P} + \rho_f \vec{g} + \mu \nabla^2 \vec{v}_f \quad (1)$$

$$\nabla . \overrightarrow{v}_f = 0 \quad (2)$$

Where ρ_f is the density of blood, $\overrightarrow{v}$ Velocity of the fluid phase, P is the pressure of blood, and μ is the dynamic viscosity. The rheology of blood was assumed to be a Newtonian fluid and rigid-wall conditions were applied. The problem was assumed to be a steady state and was solved using the semi-implicit method for the pressure-linked equation (SIMPLE) algorithm to resolve pressure-velocity coupling using the simpleFoam solver in OpenFOAM.

2.1.2 Modelling Particle Transport (Lagrangian Particle Tracking).

The particle transport was modelled using the Lagrangian Particle Tracking (LPT) solver particleFoam in OpenFOAM. The particle trajectories were predicted by the equations of Newton's second law in the known fluid domain obtained from the simpleFoam solver.

$$\frac{dv_p}{dt} = \frac{\sum F}{m_p} = \frac{F_{drag} + F_{gravity}}{m_p} \quad (3)$$

Where, m_p is the mass of the particle and v_p is the particle velocity. The forces acting on individual particles were determined by Newton's second law of motion. $\sum F$ is the summation of the considered dominant forces in this case - hydrodynamic drag (F_{drag}) and gravity force ($F_{gravity}$). Other forces were neglected due to problem specification and computational demand. The drag force is defined in equation 4 [20].

$$F_{drag} = m_p \frac{\rho_p d_p^2}{18\mu} \frac{24}{C_D Re_p} \left(v_f - v_p\right) \quad (4)$$

Where, C_D is the drag coefficient, ρ_p is the density of the particle, Re_p is the particle Reynolds number, $(v_f - v_p)$ is the relative velocity between the fluid and the particle. In this study, the laminar flow regime with micron-sized spherical particles was considered. Hence, the particle Reynolds number was assumed to be less than 1000, and

ICCS Camera Ready Version 2026
To cite this paper please use the final published version:
DOI: 10.1007/978-3-032-29915-4_1

the Schiller-Naumann correlation was applied to model the viscous and inertial effects accurately. The drag coefficient C_D [20] is now expressed in equation 5.

$$C_D = \frac{24}{Re_p}\left(1 + 0.15Re_p^{0.687}\right), \quad for\ Re_p < 1000 \tag{5}$$

The gravity force is defined as

$$F_{gravity} = \frac{4}{3}\pi r_p^3 \rho_p g \tag{6}$$

The Stokes number (St) [21] is a dimensionless number that is significant in defining the behavior of particles dispersed in the flow. The Stokes number is represented in equation (7)

$$St = \frac{\rho_p d_p^2 v_f}{18\mu l_0} \tag{7}$$

here the characteristic dimension l_0 is defined by the inlet diameter of the domain.

2.2 Computational Domain

The geometric parameters and boundary conditions for both Y and T bifurcation are described in Table 1 and Figure 3. The inlet velocity was examined at three levels (0.212 m/s, 0.30 m/s, and 0.36 m/s) to vary the Reynolds number from approximately 150 to 1000 while maintaining the flow in the laminar regime. The particle density varied across three levels (1050 kg/m^3, 1100 kg/m^3, 1150 kg/m^3) to investigate the effects of neutrally buoyant, positively buoyant, and negatively buoyant particles. For the Y bifurcation, Θ_1 was varied between angles 50°, 70°, 90°, 110°, 150° and for the T bifurcation, Θ_2 was varied between 50°, 70°, 90°, 110°, 130°, 150° respectively. The diameters were varied with different combinations. For the Y bifurcation, D was varied over 10 levels, and for the T bifurcation, 7 levels were used, ranging from 1.5 to 8 mm. Constant length (*L1* (60 mm), *L2* (25 mm), *L3* (25 mm)) was retained.

Table 1. Geometric parameters

Y Bifurcation		T Bifurcation	
Parameter	Notation	Parameter	Notation
Inlet Diameter	I	Inlet Diameter	I
Outlet 01 Diameter	D_1	Outlet 01 Diameter	D_1
Outlet 02 Diameter	D_2	Outlet 02 Diameter	D_2
Parent Vessel Length	L_1	Parent Vessel Length	L_1
Daughter Vessel 01 Length	L_2	Daughter Vessel 01 Length	L_2
Daughter Vessel 02 Length	L_3	-	-
Bifurcation Angle	Θ_1	Bifurcation Angle	Θ_2

ICCS Camera Ready Version 2026
To cite this paper please use the final published version:
DOI: 10.1007/978-3-032-29915-4_1

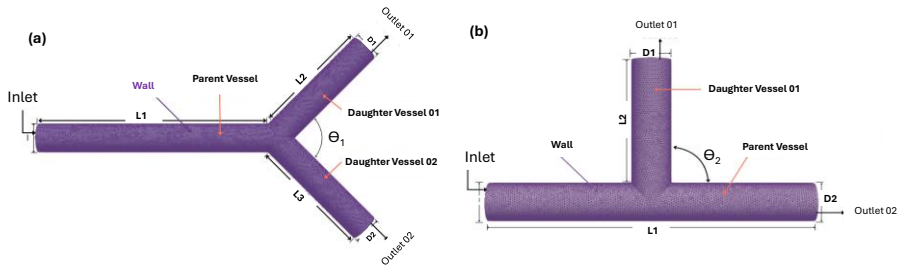

Fig. 3. Representative computational domains used for CFD simulations: (a) Y Bifurcation, (b) T Bifurcation. Gravity was oriented downwards in the vertical plane.

The mesh was generated using tetrahedral elements with inflation layers to accurately capture the quantities of interest at the outlets, resulting in 776,384 elements and an average cell size of 0.34 mm. A grid convergence study was performed to confirm that the results were independent of the mesh construction at this scale. The rheology of blood was assumed to be a Newtonian fluid [22] with a density of 1100 kg/m^3 and a dynamic viscosity of 0.003 Pa.s [23]. A total of ten thousand spherical particles with 1.6 µm diameter were injected at the inlets of both the Y- and T-bifurcation geometries, and a one-way coupling assumption was adopted for fluid particle interaction with ideal wall collision.

2.3 Machine Learning Implementation

To reduce the complexity and computational cost of simulations across a large vascular network, our approach builds the training dataset by varying the geometry and boundary conditions of Y- and T-shaped bifurcation fragments. The variations in geometry and boundary conditions are shown in Table 1. The results obtained from these single bifurcations are used to build the training dataset and generate predictions for generation 01 bifurcations. The predictions from generation 01 bifurcations were used as inputs for generation 02 bifurcation fragments to create a larger network, as illustrated in Figure 1. The dataset obtained from the simulation results was used to train three ML models: Linear Regression (LR), k-Nearest Neighbour (kNN), and Random Forest Regression (RFR).

The metrics used to compare the performance of the ML algorithms were the Mean Squared Error (MSE), Root Mean Squared Error (RMSE), Mean Absolute Error (MAE) and the Coefficient of Determination (R^2).

$$MSE = \frac{1}{n}\sum_{i=1}^{n}(y_i - y_i')^2 \tag{8}$$

$$RMSE = \sqrt{MSE} \tag{9}$$

$$MAE = \frac{1}{n}\sum_{i=1}^{n}|y_i - y_i'| \tag{10}$$

ICCS Camera Ready Version 2026
To cite this paper please use the final published version:
DOI: 10.1007/978-3-032-29915-4_1

$$R^2 = 1 - \frac{\sum_{i=1}^{n}(y_i - y_i')^2}{\sum_{i=1}^{n}(y_i - y'')^2} \quad (11)$$

Where n is the number of observations, y_i is the actual value and y_i' is the predicted value, and y'' is the mean of actual values.

The performance of our scalable prediction model was compared with flow simulation results from the multi-bifurcation domain P1, illustrated in Figure 4, and the realistic hepatic artery domain of [24]. The velocity and exit fractions from outlets 01, 02, 03, and 04 were the parameters used to compare ML predictions with CFD-LPT simulations on P1. Table 2 summarises the output parameters in the study

Table 2. Output parameters of interest

Parameter	Notation	Parameter	Notation
Velocity (outlet 1)	V1	Exit fraction (outlet 1)	EF1
Velocity (outlet 2)	V2	Exit fraction (outlet 2)	EF2
Velocity (outlet 3)	V3	Exit fraction (outlet 3)	EF3
Velocity (outlet 4)	V4	Exit fraction (outlet 4)	EF4

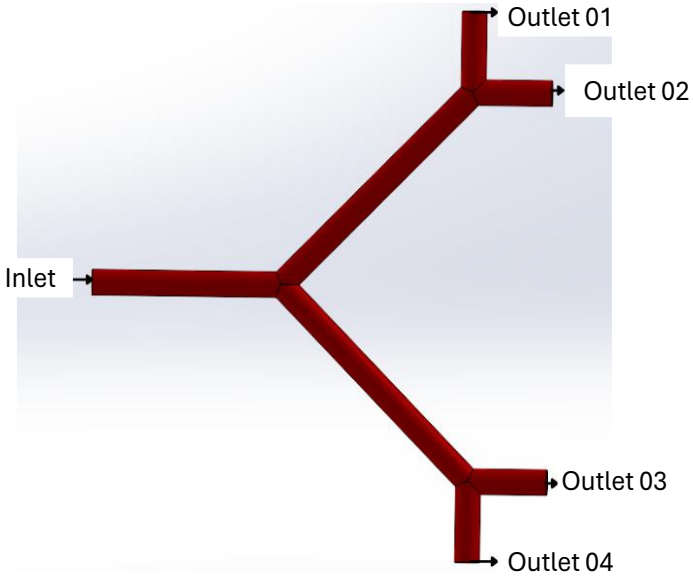

Fig. 4. (Multi-bifurcation) Model P1, which is used to evaluate the performance of the ML framework.

ICCS Camera Ready Version 2026
To cite this paper please use the final published version:
DOI: 10.1007/978-3-032-29915-4_1

3 Results

3.1 Validation

To validate the accuracy of the simpleFoam and particleFoam solvers, the results were compared with those of the in-vitro experiments by Bushi et al. [23] and the computational studies of Param et al. [25] in a replicated domain of a Y bifurcation (specific details can be found in the supplementary dataset). Steady-state condition was used for the simulation of the fluid phase, and a Reynolds number (*Re*) of 500 was imposed at the inlet. The flow ratio (*Q1/Q2*) was varied at the outlets by varying the pressure at outlet 02 and retaining constant pressure at outlet 01, where *Q1* and *Q2* are the flow rates in outlets 01 and 02. Ten thousand neutrally buoyant spherical particles were injected at the inlet with particle diameters of 0.6 mm, assuming one-way coupling between particle and fluid. The exit fraction at the outlets was calculated by equation (12)

$$Exit\ Fraction\ (\%) = \frac{Number\ of\ particles\ exiting\ from\ an\ outlet}{Number\ of\ injected\ particles} \quad (12)$$

A comparison of the results obtained from the current study and the literature is shown in Figure 5. The results obtained from present study showed a similar trend to the literature validating the accuracy of the solver.

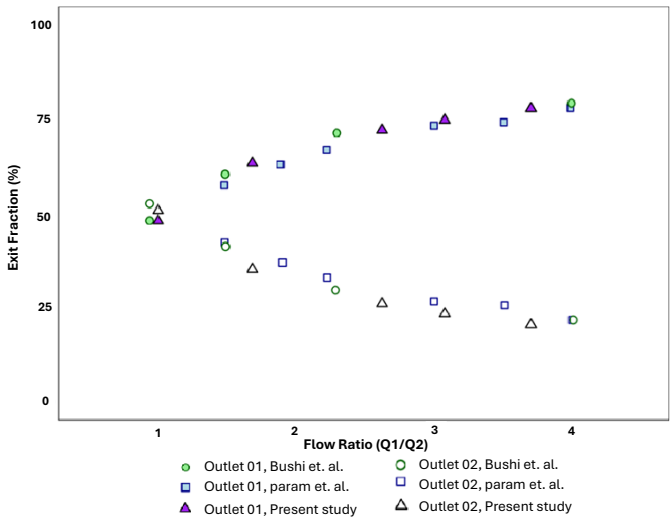

Fig. 5. Comparison of particle exit fraction between the present study and the experiments of Param et al. [25] and Bushi et al [23].

3.2 Performance of ML algorithms for single bifurcations

The CFD-LPT results were used to train ML models for predicting the output parameters (velocity, particle exit fraction) for a single bifurcation. Detailed results on CFD-

ICCS Camera Ready Version 2026
To cite this paper please use the final published version:
DOI: 10.1007/978-3-032-29915-4_1

LPT simulations are available in the data availability section. Table 3 demonstrates the performance of ML algorithms for generation 01 bifurcations. The best overall performance in predicting four output parameters (velocity at outlets 01 and 02 and exit fraction at outlets 01 and 02) for a generation 01 bifurcation was achieved with the RFR algorithm. Slightly weaker performance was observed for both kNN and LR, though both had most R^2 values above 0.98. The performance of the ML algorithms was further analysed by comparing CFD-LPT simulation results with ML predictions. Figure 6 compares the predicted velocity at outlet 01 from the ML approach and CFD-LPT simulations using different ML algorithms. As shown in Figure 6, the predicted values from the RFR algorithm closely follow the actual values (CFD-LPT), as expected, given that the ML algorithms were trained on data from generation 01 bifurcations. kNN began showing slight deviations, and LR had the lowest accuracy of the three algorithms.

Table 3. Performance metrics of ML algorithms

Algorithm	Parameter	MSE	RMSE	MAE	R^2
LR	V1	0.0002	0.0143	0.0116	0.9697
	V2	8.8e-05	0.0093	0.0069	0.9840
	EF1	9.0008	3.0001	2.4049	0.9913
	EF2	9.7504	3.1225	2.5295	0.9914
RFR	V1	1.1E-06	0.0010	0.0007	0.9998
	V2	1.8E-06	0.0013	0.0008	0.9996
	EF1	0.1748	0.4181	0.2358	0.9998
	EF2	0.2531	0.5031	0.2822	0.9997
kNN Regression	V1	8.8E-05	0.0094	0.0044	0.9869
	V2	0.0001	0.0104	0.0048	0.9803
	EF1	12.4237	3.5247	1.5920	0.9880
	EF2	12.6909	3.5624	1.6585	0.9888

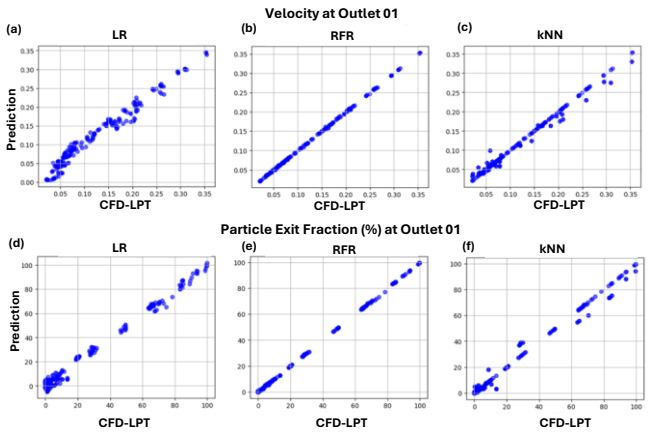

Fig. 6. Comparison of predicted and computed velocities from algorithms (a) LR (b) RFR, (c) kNN and exit fractions from algorithms (d) LR, (e) RFR, (f) kNN at outlet 01 for generation 01 bifurcations

ICCS Camera Ready Version 2026
To cite this paper please use the final published version:
DOI: 10.1007/978-3-032-29915-4_1

3.3 Performance of Scalable ML model

3.3.1 Comparison with P1

The predicted results from generation 02 bifurcations were compared with the results of CFD-LPT simulations carried out on the performance evaluation model P1 (Figure 4). Contrary to generation 01 predictions, the overall best performance in velocity prediction was observed by the LR (RMSE 0.031) and RFR (0.034) regression for generation 02 bifurcations. The worst outcome was observed by the kNN (RMSE 0.29) algorithm. LR (RMSE 6.61) and RFR (RMSE 10.49) show better performance in predicting exit fractions. The weakest performance in predicting both parameters for generation 02 bifurcations was observed by the kNN (RMSE 38.73) algorithm.

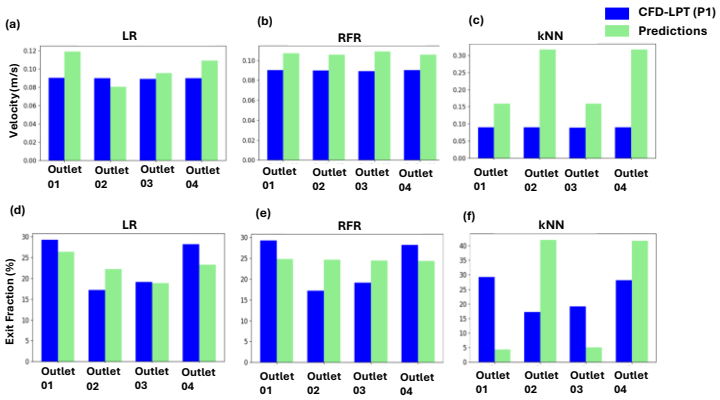

Fig. 7. Comparison of predicted and computed velocities from algorithms (a) LR, (b) RFR, (c) kNN and exit fractions from algorithms (d) LR, (e) RFR, (f) kNN at four outlets for generation 02 bifurcations

3.3.2 Comparison with literature

To evaluate the performance of our model with flow in a more realistic vasculature, we generated a representation of the hepatic arterial domain presented in Figure 8 of Umbarkar and Kleinstreuer [24]. We represented the Proper hepatic artery (PHA), right hepatic artery (RHA) and left hepatic artery (LHA) in our model as two generations of Y-bifurcations using the RFR algorithm, as it performed best in generation 01 (RMSE 0.4181 for EF1). A comparison of the results of normalised particle exit fraction at the four hepatic artery outlets found in [24] (ignoring particles exiting via the gastroduodenal artery-GDA) and the developed prediction model is shown in Table 4. Similar geometric and flow profiles to [24] were given as inputs in our prediction model. Whilst the absolute values of exit fraction are different to the 3D results obtained by Umbarkar and Kleinstreuer [24], our model correctly predicts the order of outlet exit fractions and that the D3 saw significantly greater particles exiting compared to the other outlets. This latter result was not observed in the 1D results presented by [24] in conjunction with their 3D data. Although the geometric domain is different, considering curves and

ICCS Camera Ready Version 2026
To cite this paper please use the final published version:
DOI: 10.1007/978-3-032-29915-4_1

angles, the prediction of the distribution of particles was successfully achieved using the developed prediction model.

Table 4. Comparison of our predictive model with literature results for a hepatic arterial domain. The literature data has been normalised to ignore the particles leaving via the GDA to ensure a fair comparison with our results

Outlet	Exit Fraction (%) [24] 1D model (Normalised)	Exit Fraction (%) [24] 3D model (Normalised)	Exit Fraction (%) Prediction Model (RFR)
D1	27.19	17.56	10.42
D2	20.62	21.77	18.84
D3	27.71	39.99	46.27
D4	24.49	20.68	14.34

Table 5. Comparison of Computing Requirements

Computation	Umbarkar and Kleinstreuer [24]	Our Model
1D Model	2.67 GHz CPU, 6GB RAM (Runtime 60 minutes), for four cardiac cycles)	-
3D Model	10 processors, 40 GB RAM, 3.33 GHz (Runtime 4 days), for four cardiac cycles)	60 processors, 60 GB RAM, 2.45 GHz (Runtime 9 days, for the entire campaign of CFD-LPT simulations)
ML Model		8 Processors, 32 GB RAM, 2.3 GHz (Runtime 40 seconds for single generation training and evaluation)

4 Discussion

The primary objective of our approach was to develop a prediction model using a dataset comprising CFD-LPT results from geometric and flow variations from Y- and T-bifurcation fragments, thereby reducing the need for time and resource-intensive simulations over a large domain.

All ML algorithms showed good performance on generation 01 bifurcations, as expected. However, the key challenge was predicting the output parameters for second-generation bifurcations, as the model had to make predictions in an entirely new environment that it had not encountered before and may not have been fully represented in the training data. Nonetheless, our prediction model successfully predicted the distribution of particle exit fraction in a replicated condition of a realistic geometric domain of [24], which the 1D model was unable to adequately represent. The 1D analysis reported by Umbarkar and Kleinstreuer [24] required approximately 1% of the computational time compared to 3D simulations. Although the simulations for generating the

ICCS Camera Ready Version 2026
To cite this paper please use the final published version:
DOI: 10.1007/978-3-032-29915-4_1

training dataset took significantly longer, the ML predictions required a fraction of the runtime of both the 1D and 3D models of [24] and achieved better accuracy than the 1D models. The ML based model generated the predictions in Table 4 in under 3 minutes of compute time.

The LR and RFR demonstrated the best predictive accuracy, whereas kNN showed the poorest performance in predicting particle exit fraction when compared to P1. This is primarily due to the complexity of setting up the number of neighbours (k value). A large k value risks averaging over very different target values (bad smoothing), while a small k risks fitting to local noise instead of the true trend [26].

From Figure 7, an even distribution of particles was observed from the RFR algorithm for the P1 model. This was primarily due to RFR having an R2 score of almost 0.9999 for each of the output parameters of interest, and an even distribution of particles was observed in the simulation across geometries with a D1/D2 ratio of 1. Because the P1 model has a D1/D2 ratio of 1, an even distribution was predicted. In contrast, the domain of [24] had a D1/D2 ratio of 1.20 and, therefore, a uneven distribution between exit fractions were predicted when this was used as an input to our ML model. Nonetheless, the ML model only represents the underlying patterns present within the training data. The relative order of 3D particle exit fractions seen in [24] was replicated by the predictions made by our framework.

Although full-scale 3D CFD-LPT simulations were conducted, several simplifications were considered due to computational limitations. The assumption of blood as a Newtonian fluid and rigid walls is one limitation in this study. Another limitation is the assumption of steady-state flow and the one-way coupling assumption for particle tracking. The flow behaviour was primarily governed by the geometric domain [27]. However, steady-state simulations did not capture the pulsatile characteristics of the flow, and variations in particle density had a negligible influence due to $St < 1$ under the one-way coupling assumption.

Although generation 01 prediction models showed accurate results, the results of generation 02 predictions were limited. A significant challenge in improving prediction accuracy in later generations of bifurcations is incorporating temporally and spatially varying flow profiles from the larger domain into the simulations of fragmented subdomains. A skewed velocity distribution was observed at the junction points of second-generation bifurcations when simulations were conducted on P1. Figure 8 shows the velocity distribution of model P1. As particle trajectories largely depend on the flow, this certainly affects the distribution of particle deposition. Incorporating further variation in geometric and flow parameters may include unforeseen profiles into the training dataset.

ICCS Camera Ready Version 2026
To cite this paper please use the final published version:
DOI: 10.1007/978-3-032-29915-4_1

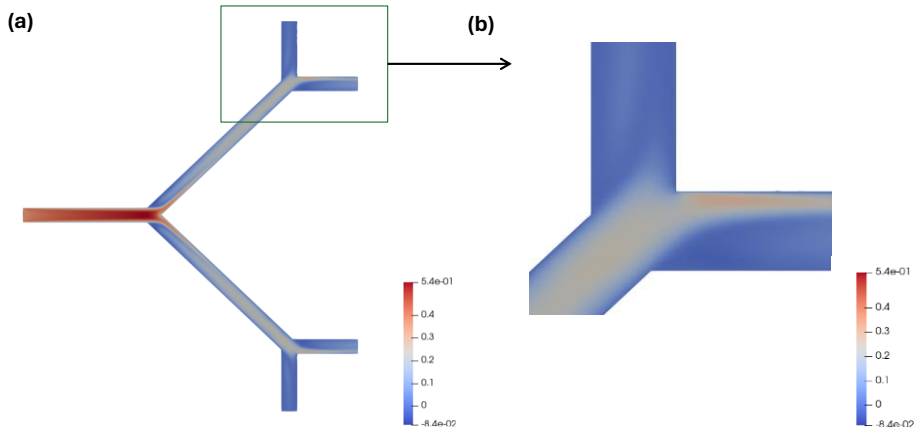

Fig. 8. Velocity distribution (x direction) of (a) model P1 and observed (b) skewed profile

As a preliminary step, the present work represents an initial approach using an ML framework. Improved data handling in the ML model would increase the efficiency of generating particle distribution predictions in large vascular networks with multiple bifurcation components. Other predictive modelling approaches, such as Artificial Neural Networks (ANNs), Convolutional Neural Networks (CNNs), and Physics-Informed Neural Networks (PINNs), remain unexplored and could offer further benefits to the presented framework. With various combinations of Y and T bifurcations, including fragments from patient-specific geometries, an entire tree of vascular network may be reconstructed. Thus, further investigation of a larger vascular network is still required.

5 Conclusion

In this paper, a scalable framework for predicting flow characteristics and particle transport in bifurcating vascular networks was constructed by training an ML model on output from 3D CFD-LPT simulations. By successively combining simulation results from smaller bifurcation variants, a larger network was represented in a modular fashion. This approach enables rapid evaluation of flow dynamics and particle transport while substantially reducing computational requirements and demonstrating improved predictive capability compared to conventional one-dimensional modelling approaches. Furthermore, our framework substantially decreases the computational burden of dataset generation by avoiding full-network simulations. Although certain limitations had to be considered, there remain several areas in which the current framework could be further refined. In our future work, we wish to incorporate the pulsatile nature of flow with more realistic vessel shapes and explore PINNs in larger networks.

Data availability. All mesh files and scripts and supplementary dataset are available at: https://github.com/Zaheenman/CFD_DPM__ML_Vascular_Repository

ICCS Camera Ready Version 2026
To cite this paper please use the final published version:
DOI: 10.1007/978-3-032-29915-4_1

Acknowledgments. We are grateful for the use of the computing resources from the Northern Ireland High Performance Computing (NI-HPC) service funded by EPSRC (EP/T022175).

Disclosure of Interests. The authors have no competing interests to declare that are relevant to the content of this article.

References

1. Nedkoff, L., Briffa, T., Zemedikun, D., Herrington, S., & Wright, F. L. Global Trends in Atherosclerotic Cardiovascular Disease. Clinical Therapeutics, **45**(11), 1087-1091, doi:https://doi.org/10.1016/j.clinthera.2023.09.020. (2023).
2. Cicha, I. The Grand Challenges in Cardiovascular Drug Delivery. [Specialty Grand Challenge]. Frontiers in Drug Delivery, Volume 1 - 2021, doi:10.3389/fddev.2021.784731. (2021).
3. Lee, B.-K. Computational Fluid Dynamics in Cardiovascular Disease. kcj, **41**(8), 423-430, doi:10.4070/kcj.2011.41.8.423. (2011).
4. Meschi, S. S., Farghadan, A., & Arzani, A. Flow topology and targeted drug delivery in cardiovascular disease. Journal of Biomechanics, **119**, 110307, doi:https://doi.org/10.1016/j.jbiomech.2021.110307. (2021).
5. Zhong, L., Zhang, J.-M., Su, B., Tan, R. S., Allen, J. C., & Kassab, G. S. Application of Patient-Specific Computational Fluid Dynamics in Coronary and Intra-Cardiac Flow Simulations: Challenges and Opportunities. [Review]. Frontiers in Physiology, Volume 9 - 2018, doi:10.3389/fphys.2018.00742. (2018).
6. Kurtcuoglu, V., & Poulikalos, D. Principles and challenges of computational fluid dynamics in medicine. In 9th MICCAI Workshop on Computational Biomechanics For Medicine, (pp. 14-22), (October 2006).
7. Malek, S., Eskandari, A., & Sharbatdar, M. Machine learning-based prediction of hemodynamic parameters in left coronary artery bifurcation: A CFD approach. Heliyon, **11**(2). (2025).
8. Alqarni, A. A., Alqarni, M., Felemban, M. F., Algahtani, F. S., Alzubaidi, M. A., & Shukr, B. S. Advanced hybrid numerical-machine learning computational study on fluid flow modeling in magnetic nanocarriers for targeted drug delivery. Case Studies in Thermal Engineering, **59**, 104497. (2024).
9. Islam, M. S., Larpruenrudee, P., Rahman, M. M., Li, G., Husain, S., Munir, A., et al. Pharmaceutical aerosol transport in airways: A combined machine learning (ML) and discrete element model (DEM) approach. Powder Technology, **448**, 120271. (2024).
10. Francis, I., & Saha, S. C. Computational fluid dynamics and machine learning algorithms analysis of striking particle velocity magnitude, particle diameter, and impact time inside an acinar region of the human lung. Physics of Fluids, **34**(10). (2022).
11. Lin, D., & Kenjereš, S. Towards fast and reliable estimations of 3D pressure, velocity and wall shear stress in aortic blood flow: CFD-based machine learning approach. Computers in Biology and Medicine, **191**, 110137. (2025).
12. Coenen, A., Lubbers, M. M., Kurata, A., Kono, A., Dedic, A., Chelu, R. G., et al. Fractional flow reserve computed from noninvasive CT angiography data: diagnostic performance of an on-site clinician-operated computational fluid dynamics algorithm. Radiology, **274**(3), 674-683. (2015).
13. Ko, B. S., Cameron, J. D., Munnur, R. K., Wong, D. T., Fujisawa, Y., Sakaguchi, T., et al. Noninvasive CT-derived FFR based on structural and fluid analysis: a comparison with

ICCS Camera Ready Version 2026
To cite this paper please use the final published version:
DOI: 10.1007/978-3-032-29915-4_1

invasive FFR for detection of functionally significant stenosis. JACC: Cardiovascular Imaging, **10**(6), 663-673. (2017).
14. Kuprat, A. P., Jalali, M., Jan, T., Corley, R. A., Asgharian, B., Price, O., et al. Efficient bi-directional coupling of 3D Computational Fluid-Particle Dynamics and 1D Multiple Path Particle Dosimetry lung models for multiscale modeling of aerosol dosimetry. J Aerosol Sci, **151**, doi:10.1016/j.jaerosci.2020.105647. (2021).
15. Longest, P. W., Bass, K., Dutta, R., Rani, V., Thomas, M. L., El-Achwah, A., et al. Use of computational fluid dynamics deposition modeling in respiratory drug delivery. Expert Opin Drug Deliv, **16**(1), 7-26, doi:10.1080/17425247.2019.1551875. (2019).
16. Dassault Systèmes: SOLIDWORKS. Dassault Systèmes, Vélizy-Villacoublay. Available at: https://www.solidworks.com last accessed 2026/04/02
17. Northern Ireland High Performance Computing (NI-HPC). Kelvin2 HPC Service. https://ni-hpc.ac.uk/Kelvin2/ last accessed 2026/04/02.
18. Jasak, H. OpenFOAM: Open source CFD in research and industry. International Journal of Naval Architecture and Ocean Engineering, **1**(2), 89-94, doi:https://doi.org/10.2478/IJNAOE-2013-0011. (2009).
19. Kramer, O. Scikit-learn. In Machine learning for evolution strategies (pp. 45-53): Springer. (2016).
20. Arefin, N. M., & Good, B. C. Emboli Transport in a Full-Length Patient-Specific Aorta: Assessment of Abdominal Organ Injury Risk During Cardiopulmonary Bypass. medRxiv, 2025.2006. 2007.25329120. (2025).
21. Ferrante, A., & Elghobashi, S. 3 - Physics of two-way coupling in particle-laden homogeneous isotropic turbulence. In S. Subramaniam, & S. Balachandar (Eds.), Modeling Approaches and Computational Methods for Particle-Laden Turbulent Flows (pp. 81-109): Academic Press. (2023).
22. De Nisco, G., Lodi Rizzini, M., Verardi, R., Chiastra, C., Candreva, A., De Ferrari, G., et al. Modelling blood flow in coronary arteries: Newtonian or shear-thinning non-Newtonian rheology? Computer Methods and Programs in Biomedicine, **242**, 107823, doi:https://doi.org/10.1016/j.cmpb.2023.107823. (2023).
23. Bushi, D., Grad, Y., Einav, S., Yodfat, O., Nishri, B., & Tanne, D. Hemodynamic Evaluation of Embolic Trajectory in an Arterial Bifurcation. Stroke, **36**(12), 2696-2700, doi:10.1161/01.STR.0000190097.08862.9a. (2005).
24. Umbarkar, T. S., & Kleinstreuer, C. Computationally efficient fluid-particle dynamics simulations of arterial systems. Communications in Computational Physics, **17**(2), 401-423. (2015).
25. Khalili Param, H., Tofighian, H., Mokhlesabadi, M., Nabaei, M., & Farnoud, A. Targeted drug delivery during radioembolization in a comprehensive hepatic artery system: A computational study. Computers & Mathematics with Applications, **135**, 193-205, doi:https://doi.org/10.1016/j.camwa.2023.02.007. (2023).
26. Zhang, S. Challenges in KNN Classification. IEEE Transactions on Knowledge and Data Engineering, *PP*, 1-1, doi:10.1109/TKDE.2021.3049250. (2021).
27. Geers, A., Larrabide, I., Morales, H., & Frangi, A. Comparison of steady-state and transient blood flow simulations of intracranial aneurysms. In 2010 Annual International Conference of the IEEE Engineering in Medicine and Biology, *2010* (pp. 2622-2625): IEEE

ICCS Camera Ready Version 2026
To cite this paper please use the final published version:
DOI: 10.1007/978-3-032-29915-4_1